Influence of Carbonic Anhydrase Activity in Terrestrial Vegetation on the ^{18}O Content of Atmospheric CO_2

Jim Gillon and Dan Yakir*

The oxygen-18 (^{18}O) content of atmospheric carbon dioxide (CO_2) is an important indicator of CO_2 uptake on land. It has generally been assumed that during photosynthesis, oxygen in CO_2 reaches isotopic equilibrium with oxygen in ^{18}O-enriched water in leaves. We show, however, large differences in the activity of carbonic anhydrase (which catalyzes CO_2 hydration and ^{18}O exchange in leaves) among major plant groups that cause variations in the extent of ^{18}O equilibrium (θ_{eq}). A clear distinction in θ_{eq} between C_3 trees and shrubs, and C_4 grasses makes atmospheric $C^{18}OO$ a potentially sensitive indicator to changes in C_3 and C_4 productivity. We estimate a global mean θ_{eq} value of ~0.8, which reasonably reconciles inconsistencies between ^{18}O budgets of atmospheric O_2 (Dole effect) and CO_2.

The rate of increase of the concentration of atmospheric CO_2 is, on average, only about half of that expected on the basis of rates of fossil fuel emissions (*1*, *2*). The ocean and the land biosphere must absorb the CO_2 not accumulated in the atmosphere. Using ^{13}C in CO_2 (*3*) and atmospheric O_2/N_2 ratios (*4*), direct estimates of the respective land and ocean sinks have been produced. On land, better understanding of CO_2 sinks and sources requires the ability to distinguish between CO_2 uptake in photosynthesis and release in respiration. The ^{18}O content of atmospheric CO_2 was shown to be a powerful tracer in this respect (*5*–*8*). The use of ^{18}O relies on the dissolution of CO_2 in water, allowing CO_2-H_2O oxygen exchange to occur. Water in leaves is highly enriched in ^{18}O, relative to soil water, owing to evaporative fractionation (*9*, *10*). Consequently, CO_2-H_2O exchange in leaves (associated with photosynthesis) or in soil (associated with soil respiration) produces contrasting ^{18}O signals in the CO_2 that is released to the atmosphere (*5*–*8*). Because the enzyme carbonic anhydrase (CA) is present in all plant leaves and rapidly catalyzes CO_2 hydration and isotopic exchange, in spite of the short residence time of CO_2 in leaves, it has generally been assumed that CO_2 involved in photosynthesis is nearly completely relabeled by ^{18}O-enriched leaf water. We directly tested this primary assumption and show that large variations in CA activity among plants result in a pervasive disequilibrium between leaf water and atmospheric CO_2 that must be considered in global ^{18}O budgets of atmospheric CO_2.

The ^{18}O content of atmospheric CO_2 is usually considered in the context of the global atmospheric $C^{18}OO$ budget (*5*, *6*, *8*):

$$\begin{aligned} c_a(d\delta_a/dt) &= F_f(\delta_f - \delta_a) + F_{oa}(\delta_o - \delta_a) \\ &\quad + a_w(F_{ao} - F_{oa}) + F_I(\delta_s - \delta_a) \\ &\quad + F_R(\delta_s - \delta_a - a_{eff}) + F_A\Delta_A \qquad (1) \end{aligned}$$

where c_a is the concentration of atmospheric CO_2, and F_{oa}, F_{ao}, F_R, F_f, and F_A are the gross fluxes of CO_2 between ocean and atmosphere, soil respiration, anthropogenic emission (due mainly to fossil fuel and biomass burning and land-use changes), and plant assimilation [where F_A = GPP (gross primary productivity)], with their respective isotopic composition (δ_x) and the associated kinetic isotopic fractionations a_w, a_{eff} across the ocean and soil surfaces. F_I is a soil invasion term due to diffusion of atmospheric CO_2 into and out of soils, allowing for exchange with soil water with no net CO_2 flux (*11*). Δ_A is the ^{18}O discrimination during plant assimilation [(*6*) and see below], which is highly sensitive to the isotopic equilibrium assumption tested here. Notably, similar ^{18}O budgets are also constructed for atmospheric O_2 and which also involve uncertainties associated with the biological fractionations [generally termed the Dole effect (*9*, *10*, *12*, *13*)]. For ^{18}O budgets of both CO_2 and O_2 (Eq. 1 or its O_2 equivalent), a key element is the contribution of the distinct plants term, due to ^{18}O enrichment of leaf water relative to soil (and ocean) water, and the required consistency in this term for both isotopic budgets.

We conducted a survey of CA activity and CO_2 exchange rates in 52 species. This range included all major plant groups (trees, shrubs, herbs, and grasses) and both main photosynthetic types (C_3 and C_4 pathways). Trees and shrubs were collected from the Jerusalem Botanic Gardens, which houses a collection of species from all continents and most ecosystems. Herbaceous species were collected at the Weizmann campus. Leaf samples (n = 3 per species) were assayed for maximal CA activity, according to the method in (*14*). In vivo CA hydration rates, CA_{leaf}, are lower, owing to low CO_2 concentrations at the site of CO_2-H_2O exchange in leaves (c_{cs}) (*15*). We used the maximal CA activity and c_{cs} values obtained from leaf-scale gas-exchange measurements of the same plant species to estimate CA_{leaf} (corrected also for leaf temperature).

The most striking feature of the survey [Fig. 1A and supplementary Web information (*16*)] was the low CA hydration rates (CA_{leaf}) observed in C_4 grass species and in particular in C_4 grasses, consistent with observations in preliminary studies on CA activity in plant leaves (*17*, *18*). Mean CA_{leaf} in C_4 species (80 $\mu mol\ CO_2\ m^{-2}\ s^{-1}$) was four times lower than in the next highest group. Among C_3 groups, mean CA_{leaf} for trees and shrubs was by far the highest (1350 $\mu mol\ CO_2\ m^{-2}\ s^{-1}$ compared with an average of 400 to 700 $\mu mol\ CO_2\ m^{-2}\ s^{-1}$ for the other groups). Intra- and interspecific differences in CA activity may vary with climatic and environmental conditions (*19*). However, on the basis of the consistency of these data with preliminary data elsewhere on C_3 versus C_4 differences, and with emerging physiological explanations of high and low CA activity, respectively (*17*, *19*), these results probably reflect the broad differences in CA activity among the major plant groups (Fig. 1).

The definition of isotopic equilibrium, θ_{eq}, developed from work on ^{18}O exchange in the CO_2/HCO_3^- reaction (*20*), was described (*14*) as

$$\theta_{eq} = 1 - e^{-k\tau/3} \qquad (2)$$

where $k\tau$ (the number of hydration and dehydration reactions per molecule of CO_2 dissolved in the leaf medium) is the product of the CA rate constant, k, and the residence time of CO_2 inside the leaf, τ. This relationship has been confirmed by comparison of θ_{eq} determined both from CA activity and leaf-scale measurements of ^{18}O discrimination (*21*). In physiologically measurable terms, $k\tau = CA_{leaf}/F_{al}$, where CA_{leaf} was obtained as above and F_{al}, the unidirectional CO_2 flux from atmosphere to leaf, was calculated from leaf-scale gas-exchange measurements under saturating light levels (*22*). We observed opposing trends for in vivo CA hydration rates and atmosphere-leaf CO_2 flux (Fig. 1A) that amplified plant group differences in θ_{eq}, such that C_4 grasses (low CA_{leaf}, high F_{al})

Department of Environmental Science and Energy Research, Weizmann Institute of Science, Rehovot 76100, Israel.

*To whom correspondence should be addressed. E-mail: dan.yakir@weizmann.ac.il

had by far the lowest mean extent of isotopic equilibrium (Fig. 1B). This is in contrast to the θ_{eq} values close to 1 found in C_3 plant groups ($\theta_{eq} > 0.95$ in 26 of the 39 C_3 species) (*16*). These measurements of θ_{eq}, spanning the entire range between 0 and 1, are in marked contrast to the common assumption that exchange between leaf CO_2 and leaf water is nearly complete (*5–8*, *23–28*).

A global view of the geographical distribution of variations in CA activity and the extent of isotopic equilibrium in leaves (Fig. 2) is obtained by applying our θ_{eq} values to corresponding plant groups described in 1° by 1° vegetation maps of 15 plant groups (*29*). This reveals a predominance of low θ_{eq} in the northern and southern subtropics (10° to 30°), where C_4-based ecosystems, such as savanna and grassland habitats, dominate (Fig. 2). To obtain a first approximation of the extent of global disequilibrium, the above map of θ_{eq} was made compatible with that used in the SiB2 land biosphere model (*8*). We define three "mega-groups" with distinct θ_{eq} values for the terrestrial vegetation on the basis of the SiB2 vegetation groups (*30*) (see Table 1). Then, the value of θ_{eq} at each grid point is weighted by F_{la}, the backflux of CO_2 from plants to atmosphere, where $F_{la} = GPP \cdot \varepsilon$, $\varepsilon = c_{cs}/(c_a - c_{cs})$, and *GPP* (gross primary productivity) and ε are obtained from the SiB2 global simulation. Using this approach we estimate global mean θ_{eq} between CO_2 and plant leaf water to be 0.78 (Table 1). Put simply, this indicates that, in contrast to current assumptions, only ~80% of the diffusional CO_2 backflux from plants to the atmosphere reflects the leaf water signal relevant to atmospheric $C^{18}OO$ budgets. Ignoring such incomplete equilibrium could result in about 20% underestimation of the gross CO_2 exchange with plants derived from atmospheric measurements of $\delta^{18}O$ values (*5–8*). The relative contribution from each vegetation type to the global θ_{eq} signal is calculated as $[GPP \cdot \varepsilon \cdot (1 - \theta_{eq})]_{vegtype}/[GPP \cdot \varepsilon \cdot (1 - \theta_{eq})]_{globe}$, where the numerator uses parameters for each vegetation type, and the denominator uses the global value. Consistent with Fig. 2, this analysis indicates that most of the ^{18}O disequilibrium effect is due to C_4 grassland (~54%) and C_3 grassland (~29%). The global perspectives discussed above (vegetation map and weighting by gross CO_2 fluxes) show that C_4-dominated vegetation has an overwhelming effect in reducing ^{18}O exchange between CO_2 and leaf water.

Considering the atmospheric ^{18}O budget in the context of Eq. 1, the ^{18}O signal of terrestrial plants is represented by an apparent discrimination against ^{18}O during photosynthesis, Δ_A (*6*). This was recently adapted to include θ_{eq} (*14*, *21*) for which a simplified version is

$$\Delta_A = \bar{a} + \varepsilon[\theta_{eq}(\delta_e - \delta_a) - (1 - \theta_{eq})\bar{a}/(\varepsilon + 1] \qquad (3)$$

where $\bar{a}$ is the mean diffusional fractionation of $C^{18}OO$ from air to leaf, $\varepsilon = c_{cs}/(c_a - c_{cs})$ as above, and δ_e refers to the $\delta^{18}O$ of CO_2 in equilibrium with chloroplast water. Recent global budgets constructed with Eq. 1 estimate Δ_A to be 13.7‰ (*6*) and 9.0‰ (*8*). When our global mean estimate of $\theta_{eq} = 0.78$ is used, instead of assuming $\theta_{eq} = 1$ (as was commonly done in the original analyses), equivalent values for Δ_A can be derived only by modifying ε (i.e., leaf internal CO_2 concentrations), δ_e (i.e., leaf water $\delta^{18}O$), or both, assuming that δ_a is precisely measured and $\bar{a}$ is theoretically well constrained. These values are not directly measured and involve marked uncertainties. Focusing, for example, on the analysis of (*6*), we show that modifying ε values alone would require physiologically

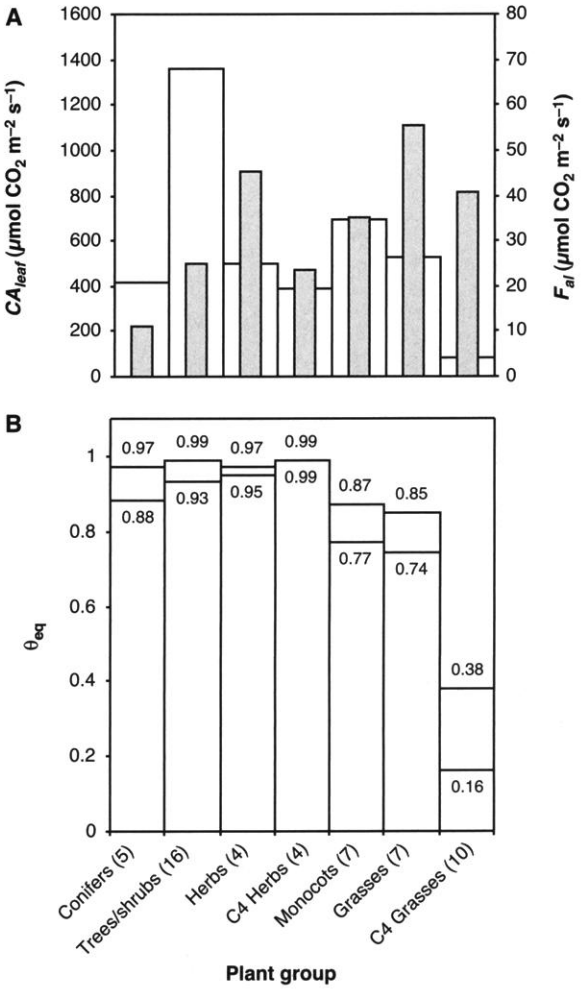

Fig. 1. (**A**) The activity of CA within leaves (CA_{leaf}, open bars) and rates of gross CO_2 flux into leaves (F_{al}, shaded bars) and (**B**) extent of isotopic equilibrium, θ_{eq}, between CO_2 and water in plant leaves. Bars represent the mean of the data, grouped according to major taxonomic or physiological category (the number of species sampled for each group is given in parentheses). Mean values of θ_{eq} were determined for the entire group, with or without outlier species where θ_{eq} was >1 SD above or below the group mean (hence the two values shown in the figure), to allow for the potential effect of nonrepresentative species. Note that although $\theta_{eq} \approx 1$ for C_4 herbs, this group contributes negligibly to global GPP (*32*) and is ignored elsewhere. To calculate θ_{eq} according to Eq. 2, we derived in vivo CA activity for each species from assays on leaf CA extracts at 17.5 mM CO_2. This was corrected to a CO_2 concentration within aqueous leaf media (from applying Henry's law to c_{cs} at measured leaf temperatures), assuming $K_m = 2.5$ mM for C_4 plants (*17*) and 5 mM for C_3 species (*41*). These were corrected to leaf temperature by adopting $Q_{10} = 2$ (*17*). The gross CO_2 influx, F_{al}, was derived from gas-exchange measurements as $F_{al} = F_{la} + A$, where $F_{la} = A \cdot \varepsilon$ and $\varepsilon = c_{cs}/(c_a - c_{cs})$. Fick's law was applied to calculate c_{cs} by $A = g_w(c_i - c_{cs})$, assuming an internal CO_2 conductance of 0.5 and 1.2 mol m^{-2} s^{-1} for woody and herb species, respectively (*14*).

Table 1. Mean values of isotopic equilibrium (θ_{eq}) for grouped vegetation types weighted by the respective CO_2 fluxes (from SiB2 land-biosphere simulation). CO_2 concentrations inside chloroplasts were taken from the SiB2 model and adjusted by +18 parts per million to account for CO_2 concentration gradient between the site of CO_2 fixation and CO_2 hydration (*14*). Numbers in parentheses refer to the equilibrium values derived from mean θ_{eq} values, excluding outliers. Allowing for the effect of outliers makes no difference to the overall global θ_{eq}.

Vegetation	GPP (Pmol C a^{-1})	C_{cs} (ppm)	εGPP (Pmol C a^{-1})	θ_{eq}
Forest/shrub	3.86	198	4.72	0.93 (0.99)
C_3 grassland	1.75	188	1.92	0.70 (0.71)
C_4 grassland	2.80	160	2.25	0.52 (0.37)
Global	8.4	185	8.9	0.78 (0.77)

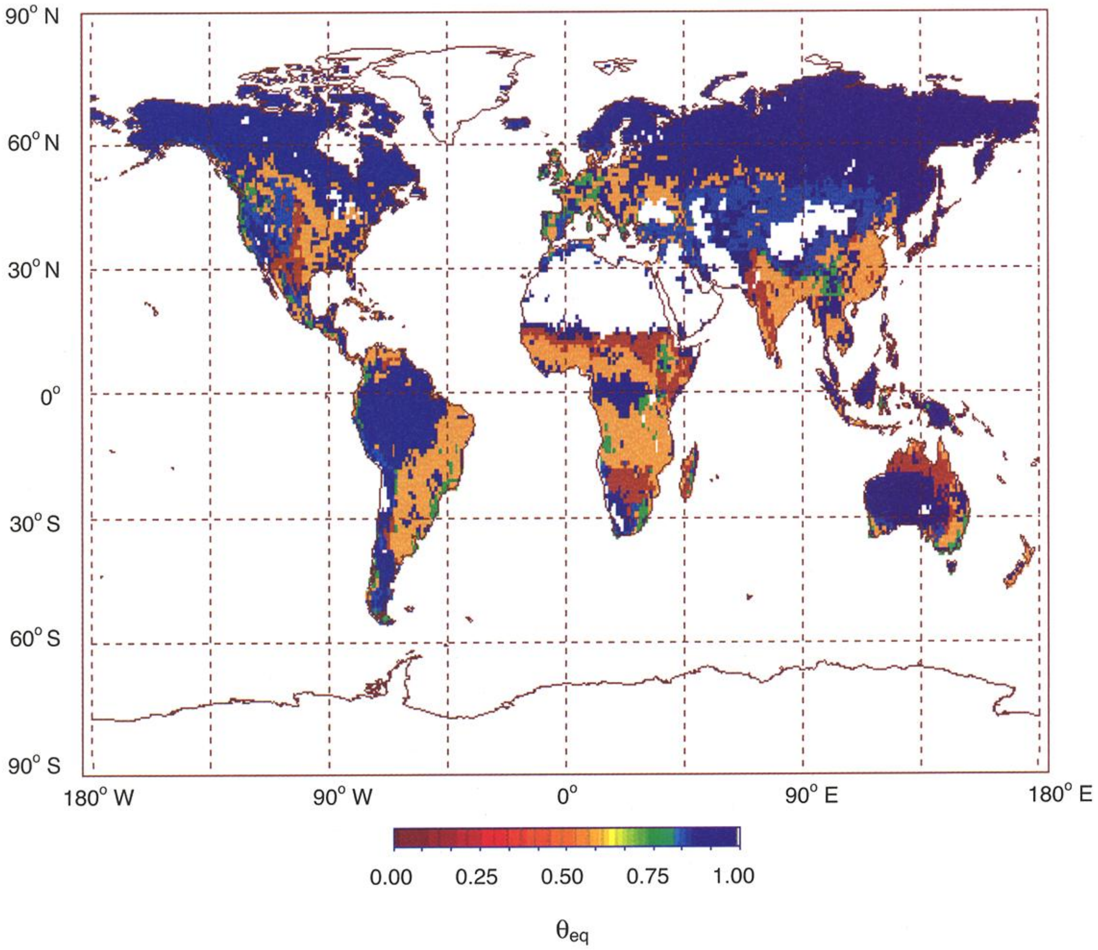

Fig. 2. Estimated geographical distribution of the extent of isotopic equilibrium, θ_{eq}, for global vegetation types (*29*). These were inferred from mean θ_{eq} of the seven plant groups in Fig. 1. Values were directly applied where vegetation types were equivalent to the groupings in Fig. 1 (i.e., coniferous forest, broadleaf forest, C_3 grassland, and C_4 grassland) or merged from two appropriate groups [mixed forest, θ_{eq} = 0.91 (0.98); forest and C_3 grassland, θ_{eq} = 0.92 (0.84); forest and C_4 grassland, θ_{eq} = 0.69 (0.55)]. The value of θ_{eq} for cultivated land [0.69 (0.55)] was based on a 40:40:20 weighting for C_4:C_3 grasses:C_3 dicots; shrubs/bare ground and tundra were assumed to comprise C_3 herbs and shrubs. The above numbers in parentheses refer to isotopic equilibrium on the basis of mean θ_{eq}, excluding outliers (i.e., the higher values in Fig. 1 with the exception of C_4 grasses, where the lower value is that without outliers). Excluding outliers increases the potential difference between vegetation group θ_{eq} and is plotted in Fig. 2 to demonstrate the largest potential range of θ_{eq}, although in the quantitative analyses, mean values of all data are applied.

unrealistic values (Fig. 3A) compared with what is known from leaf-scale studies. Figure 3A indicates that including θ_{eq} in the calculations makes Δ_A considerably less sensitive to uncertainties in ε. Estimated values of δ_e, however, could be increased by ~3‰ (Fig. 3B) and remain within current bounds on the predicted global mean value of ^{18}O in leaf water. This is exactly what is required to reconcile the long-standing differences between δ_e estimates derived from CO_2 studies (3.3 to 4.4‰) (*6*, *8*) and from O_2 studies (about 3 to 8.8‰) (Dole effect) (*9*, *10*, *12*, *13*). Notably, compensating for θ_{eq} = 0.78 by revising δ_e estimates in (*6*) brings δ_e into quantitative agreement with estimates of ~8‰ obtained from most recent models of the Dole effect (*31*).

The ^{18}O disequilibrium effect is likely to have even wider implications for biogeochemical and climate-change research. For example, using Eq. 3 and typical values for C_3 plants (c_{cs} ~200, θ_{eq} ~0.93) and C_4 plants (c_{cs} ~140, θ_{eq} ~0.38), a distinction of about 8‰ in Δ_A values is obtained (Δ_A ~15 or ~7‰ for C_3 and C_4, respectively). This makes ^{18}O of atmospheric CO_2 a sensitive indicator of changes in C_4 contributions to GPP, at a time when two large-scale processes are expected to influence it. First, the rapid increase in atmospheric CO_2 is expected to greatly disadvantage C_4 plants (*32*, *33*). Recent modeling indicates that the global land area favoring C_4 plants after of a doubling of atmospheric CO_2 could be completely eliminated (*33*). Assuming current estimates of C_4 productivity [~25% of GPP on land; (*34*)] and no net change in total productivity, a rough estimate of the upper limits of the associated ^{18}O effect indicates a potential forcing of 30 Pg C × 8‰ = 240 Pg ‰. Assuming that this elimination of C_4 plants occurs after a doubling of the present atmospheric CO_2 pool (2 × 750 Pg C), the corresponding change in atmospheric $C^{18}OO$ could approach ~0.2‰, a signal 10 times that of current analytical precision (*35*).

In contrast, large-scale land-use changes normally result in the conversion of C_3 forests to crops and grasslands (with a large C_4 component). It is estimated (*36*) that ~4.5 Pg C year^{-1} is released as a result of deforestation, which is offset by ~3 Pg C year^{-1} that is reabsorbed as a result of abandonment and regrowth (with a net release of ~1.5 Pg C year^{-1}). Abandonment and regrowth are likely to have large grassland and C_4 components. This is because, first, forest recovery can take 50 years or longer (*36*, *37*), which is preceded by grassland/C_4 productivity; second, the increasing rate of turnover in land use does not allow full forest recovery in any case (*36*, *38*). Roughly estimating an upper limit for the ^{18}O signal involved, we assume that reabsorption of about 2 Pg C year^{-1} associated with abandonment, regrowth, and newly introduced cropland (the latter involves ~10^7 hectare year^{-1} and consequently ~0.2 Pg C year^{-1}) carries a C_4-like signal. This yields an atmospheric forcing of 2 × 8 = 16 Pg ‰ year^{-1}, or a possible trend of ~0.02‰ year^{-1} in atmospheric CO_2 (under current CO_2 concentrations). Although close to the detection limit, such a signal may be observed better on regional or local scales. Because the lifetime of ^{18}O in atmospheric CO_2 is several years, this signal could accumulate and produce a secular (decreasing) trend in the ^{18}O of atmospheric CO_2. This could help explain the trend of about −0.08‰ per year that was observed during most of the 1990s (*39*), and for which an explanation has yet to be offered.

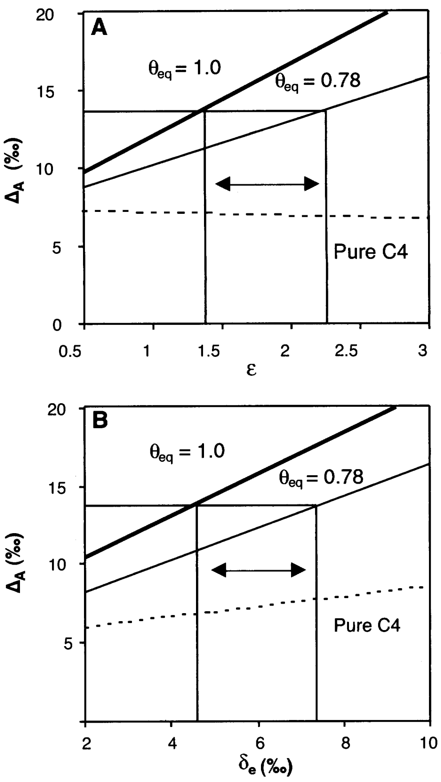

Fig. 3. Global discrimination against C^{18}OO, Δ_A, as a function of (**A**) ε values and (**B**) leaf-water δ^{18}O values. Discrimination is calculated from Eq. 3 with parameters given in (*6*) [δ_e = 4.8‰ in (A); $\bar{a}$ = 7.4‰, ε = 1.32 in (B); +0.4‰ is included in δ_e to allow for ^{18}O fractionation between leaf water and leaf CO$_2$]. The sloping lines indicate the relationships for global vegetation with (light solid line) or without (heavy solid line) the disequilibrium effect used in the global ^{18}O budget of (*6*). Also shown for comparison is the high sensitivity of global mean Δ_A to the contribution of C$_4$ plant productivity (dashed line, ε = 0.64). The horizontal line indicates global discrimination solved from the global mass balance of C^{18}OO from (*6*). Vertical lines show how a shift in θ_{eq} from 1.0 to 0.78 can be compensated for by leaf water (realistically) or ε (unrealistically), while constrained to a constant Δ_A.

References and Notes

1. R. J. Francey *et al.*, *Nature* **373**, 326 (1995).
2. C. D. Keeling, T. P. Whorf, M. Wahlen, J. van der Plicht, *Nature* **375**, 666 (1995).
3. P. Ciais, P. P. Tans, M. Trolier, J. W. C. White, R. J. Francey, *Science* **269**, 1098 (1995).
4. R. F. Keeling, S. C. Piper, M. Heimann, *Nature* **381**, 218 (1996)
5. R. J. Francey, P. P. Tans, *Nature* **327**, 495 (1987).
6. G. D. Farquhar *et al.*, *Nature* **363**, 439 (1993).
7. D. Yakir, X. F. Wang, *Nature* **380**, 515 (1996).
8. P. Ciais *et al.*, *J. Geophys. Res.* **102**, 5873 (1997).
9. G. Dongmann, *Radiat. Environ. Biophys.* **11**, 219 (1974).
10. H. Förstel, in *Proceedings* of the *3rd International Symposium on Environmental Biogeochemistry and Geomicrobiology*, W. E. Krumbein, Ed. (Ann Arbor, MI, 1978), p. 811.
11. P. P. Tans, *Tellus* **50B**, 163 (1999).
12. M. Bender, L. D. Labeyrie, D. Raynaud, C. Lorius, *Nature* **318**, 349 (1985).
13. M. Bender, T. Sowers, L. D. Labeyrie, *Global Biogeochem. Cycles* **8**, 363 (1994).
14. J. S. Gillon, D. Yakir, *Plant Physiol.* **123**, 201 (1999).
15. c_{cs} represents the CO$_2$ concentration at the chloroplast surface, which is the limit of CA activity and is thus assumed to represent the site of CO$_2$-H$_2$O in leaves. c_{cs} is typically a midway value between those in the liquid-air interfaces and the sites of CO$_2$ assimilation inside leaves (*14*).
16. Supplementary data are available on *Science* Online at www.sciencemag.org/cgi/content/full/291/5513/2584/DC1.
17. M. D. Hatch, J. N. Burnell, *Plant Physiol.* **93**, 825 (1990).
18. E. Utsoniyama, S. Muto, *Physiol. Plant.* **88**, 413 (1993).
19. A. Makino *et al.*, *Plant Physiol. 100, 1737 (1992)*
20. G. A. Mills, H. C. Urey, *J. Am. Chem. Soc.* **62**, 1019 (1940).
21. J. S. Gillon, D. Yakir, *Plant Cell Environ.* **23**, 903 (2000).
22. The gross flux of CO$_2$ from atmosphere to leaf, F_{al}, was determined from leaf-scale measurements of net CO$_2$ assimilation, A, and c_{cs}, which are related by the expression $F_{al} = A[1 + c_{cs}/(c_a - c_{cs})]$.
23. D. Yakir, J. A. Berry, L. Giles, C. B. Osmond, *Plant Cell Environ.* **17**, 73 (1994).
24. L. B. Flanagan, S. L. Phillips, J. R. Ehleringer, J. Lloyd, G. D. Farquhar, *Aust. J. Plant Physiol.* **21**, 221 (1994).
25. T. G. Williams, L. B. Flanagan, J. R. Coleman, *Plant Physiol.* **112**, 319 (1996).
26. K. G. Harwood, J. S. Gillon, H. Griffiths, M. S. J. Broadmeadow, *Plant Cell Environ.* **21**, 269 (1998).
27. X. F. Wang, D. Yakir, M. Avishai, *Global Change Biol.* **4**, 835 (1998).
28. P. Peylin *et al.*, *Tellus* **51B**, 642 (1999).
29. R. S. Defries, J. R. G. Townshend, *Int. J. Remote Sens.* **15**, 3567 (1994).
30. Groups 1 to 5, 7, and 8, as defined in the vegetation parameterization of SiB2 (*40*), all contain trees and shrubs only, which we combine into a single group with the corresponding θ_{eq} value. Group 6 (C$_4$ groundcover and grassland) we assume has some C$_3$ component and calculate θ_{eq} from a weighting of 75:25 C$_4$ grasses:trees to allow for the presence of trees in savanna-type habitats. Group 9 (C$_3$ grassland and agriculture) we assume comprises 25:50:25 for trees:C$_3$ grasses:C$_4$ grasses; the C$_3$ and C$_4$ grasses include some C$_3$ herbs and C$_4$ grass species as crops.
31. G. Hoffmann *et al.*, in preparation.
32. J. R. Ehleringer, T. E. Cerling, B. R. Helliker, *Oecologia* **112**, 285 (1997).
33. G. J. Collatz, J. A. Berry, J. S. Clark, *Oecologia* **114**, 441 (1998).
34. J. Lloyd, G. D. Farquhar, *Oecologia* **99**, 201 (1994).
35. M. Trolier, J. W. C. White, J. R. Lawrence, W. S. Broecker, *J. Geophys. Res.* **101**, 25897 (1996).
36. R. A. Houghton, *Tellus* **51B**, 298 (1999).
37. R. H. Waring, W. H. Schlesinger, *Forest Ecosystems* (Academic Press, New York, 1985).
38. R. A. Houghton, *Bioscience* **44**, 305 (1994).
39. National Oceanic and Atmospheric Administration/Institute of Arctic and Alpine Research, www.cmdl.noaa.gov/ccg (2000).
40. P. J. Sellers *et al.*, *J. Climate* **9**, 706 (1996).
41. J. Gillon and D. Yakir, data not shown [but obtained from measurement of the Michaelis constant (K_m) on four C$_3$ species—*Hibiscus* sp., *Sonchus* sp., *Asparagus* sp., *and Apera* sp.—by assaying CA activity over a range (3 to 24 mM) of CO$_2$ concentrations].
42. We are grateful to A. S. Denning and P. Peylin for SiB2 model data, X. F. Wang for physiological data, E. Negreanu for technical help, and the Jerusalem Botanic Garden for access to their collections. Supported by a fellowship from the Leverhulme Trust, UK (J.S.G.) and by grants from the Israel Science Foundation (308/96 and 695/99) and the Minerva Foundation (D.Y.).

5 October 2000; accepted 26 February 2001
Published online 8 March 2001;
10.1126/science.1056374
Include this information when citing this paper.

Ancient Geodynamics and Global-Scale Hydrology on Mars

Roger J. Phillips,[1] Maria T. Zuber,[2,3] Sean C. Solomon,[4] Matthew P. Golombek,[5] Bruce M. Jakosky,[6] W. Bruce Banerdt,[5] David E. Smith,[3] Rebecca M. E. Williams,[1] Brian M. Hynek,[1] Oded Aharonson,[2] Steven A. Hauck II[1]

Loading of the lithosphere of Mars by the Tharsis rise explains much of the global shape and long-wavelength gravity field of the planet, including a ring of negative gravity anomalies and a topographic trough around Tharsis, as well as gravity anomaly and topographic highs centered in Arabia Terra and extending northward toward Utopia. The Tharsis-induced trough and antipodal high were largely in place by the end of the Noachian Epoch and exerted control on the location and orientation of valley networks. The release of carbon dioxide and water accompanying the emplacement of ~3 × 10^8 cubic kilometers of Tharsis magmas may have sustained a warmer climate than at present, enabling the formation of ancient valley networks and fluvial landscape denudation in and adjacent to the large-scale trough.

The western hemisphere of Mars is dominated by the Tharsis rise, a broad elevated (~10 km) region extending over 30 million square kilometers. Tharsis is the locus of large-scale volcanism and pervasive fracturing that resulted from the loading of the lithosphere, or outer elastic shell, by voluminous extrusive and intrusive magmatic deposits (*1–3*). Here we use recently acquired gravity (*4*) and topography (*5*) data from the Mars Global Surveyor (MGS) spacecraft (*6*) to determine the effect of the mass load of Tharsis on the shape and gravity field of the rest of the planet. We test the hypothesis that the deformational response to the Tharsis load is responsible for the topographic trough and the heretofore unexplained ring of negative gravity anomalies (Figs. 1 and 2A) (*7*) that surround the Tharsis rise, as well as for the major gravity and topographic highs that are